

# Tunable Electronic Properties of Multilayer Phosphorene and Its Nanoribbons

S. Soleimanikahnoj and I. Knezevic\*

Department of Electrical and Computer Engineering,  
University of Wisconsin-Madison, Madison, WI 53706, USA

(Dated: March 21, 2022)

We study the effects of a vertical electric field on the electronic band structure and transport in multilayer phosphorene and its nanoribbons. We find a massive-to-massless Dirac fermion transition along the armchair direction at a critical field  $E_c$  at which the gap closes. This transition is observable in quantum Hall measurements, as the power-law dependence of the Landau-level energy on the magnetic field goes from  $\sim (n + 1/2)B$  below  $E_c$ , to  $\sim [(n + 1/2)B]^{2/3}$  at  $E_c$ , to  $\sim [(n + 1/2)B]^{1/2}$  above  $E_c$ . Multilayer phosphorene nanoribbons (PNRs) have edge states that govern electrical conduction. We propose a double-edge-gate PNR structure that works as a quantum switch.

Phosphorene is a two-dimensional (2D) counterpart of layered black phosphorus (BP) [1, 2]. The monolayer has a direct band gap of 1.45 eV [2]. The gap decreases with increasing number of layers owing to strong van der Waals interactions, but remains direct in multilayer phosphorene [3]. In each monolayer, phosphorous atoms are covalently bonded to three nearest neighbors via  $sp^3$ -hybridized orbitals, which leads to a heavily puckered structure. As a result, the electronic bandgap of phosphorene is highly tunable by strain [4, 5] and electric field [6, 7]. In particular, applying an electric field normal to the layers reduces the band gap owing to a giant Stark effect [8]. Moreover, the puckered structure is highly anisotropic, which gives rise to the phenomena such as anisotropic electronic and thermal transport [5, 6, 9, 10], linear dichroism [9, 10], and anisotropic plasmons [11].

In this letter, we investigate the effects of a vertical electric field on the electronic properties (band structure and electronic transport) of multilayer phosphorene and its nanoribbons. In multilayer phosphorene at low fields, electrons with momenta in the zigzag direction [Fig. 1(a)] have parabolic bands, but in the armchair direction they behave as massive Dirac fermions with a gap-dependent effective mass. At a critical electric field  $E_c$ , the gap closes, and electrons exhibit a massive-to-massless Dirac fermion transition. Above  $E_c$ , there are two Dirac points, and the band structure is that of anisotropic massless Dirac fermions. This continuous massive-to-massless Dirac fermion transition could be observed in Hall measurements, as the Landau-level energy dependence on the magnetic field would change from linear below  $E_c$ , to the novel 2/3-power at  $E_c$ , to the square-root dependence above  $E_c$ . In zigzag phosphorene nanoribbons (PNRs), we show that there are twofold-degenerate bands within the bulk gap, which govern electronic transport. The associated wave functions are localized near the ribbon edges. We propose a dual-edge-gate structure that affects these midgap states and drives the conducting-to-insulating transition in PNRs, thus enabling field-effect transistor action compatible with modern nanoelectronics, and potentially leading to new PNR-based devices.

*The tight-binding model.* The band structure of multilayer phosphorene is described by a tight-binding (TB) Hamiltonian

$$H = \sum_{i,j} t_{i,j} c_i^\dagger c_j, \quad (1)$$

which was parametrized on the basis of first-principles calculation within the  $GW_0$  approximation [12]. As the TB parametrization was benchmarked for mono-, bi-, and trilayers, we restrict our study here to these three systems, but note that TB may be suitable for larger multilayers, as well. A phosphorene monolayer contains two sublayers in a puckered structure and has four atoms per unit cell. Each additional layer brings four more atoms to the unit cell [see the structure of bilayer phosphorene in Fig. 1(a)], with odd-numbered layers aligned with other odd-numbered ones, and analogously for even-numbered layers. A unit cell for bilayer phosphorene is denoted by the shaded box in Fig. 1(a). In the nearest-neighbor approximation, there are fourteen relevant tight-binding hopping parameters (Table I), ten intralayer and four interlayer. The multilayer phosphorene structure is highly anisotropic. Cutting phosphorene in the (horizontal)  $y$  direction [see Fig. 1(a)] would result in an armchair edge, while cutting along the (vertical)  $x$  direction would result in a zigzag or beard edge. We refer to the  $y$ -direction as armchair and the  $x$ -direction as zigzag.

*Band structure without an applied electric field. Massive Dirac fermions.* The band structure of trilayer phosphorene is depicted in Fig. 1(b); note the rectangular Brillouin zone (BZ) and its high-symmetry  $X$  and  $Y$  points along the  $x$  and  $y$  directions. The band gap,  $E_g$ , is at the  $\Gamma$  point and has a value of 0.85 eV. Along the zigzag direction, both the conduction band (CB) and the valence band (VB) show quadratic dependencies on the wave vector  $\mathbf{k}$  [Fig. 1(b)]. We calculate the effective masses of  $m_c = 3.18m_0$  (CB) and  $m_v = 0.84m_0$  (VB), where  $m_0$  is the free-electron rest mass. In the armchair direction, however, the dispersion has an asymptotic linear trend. To describe this highly anisotropic band structure near the band gap, we propose a low-energy two-

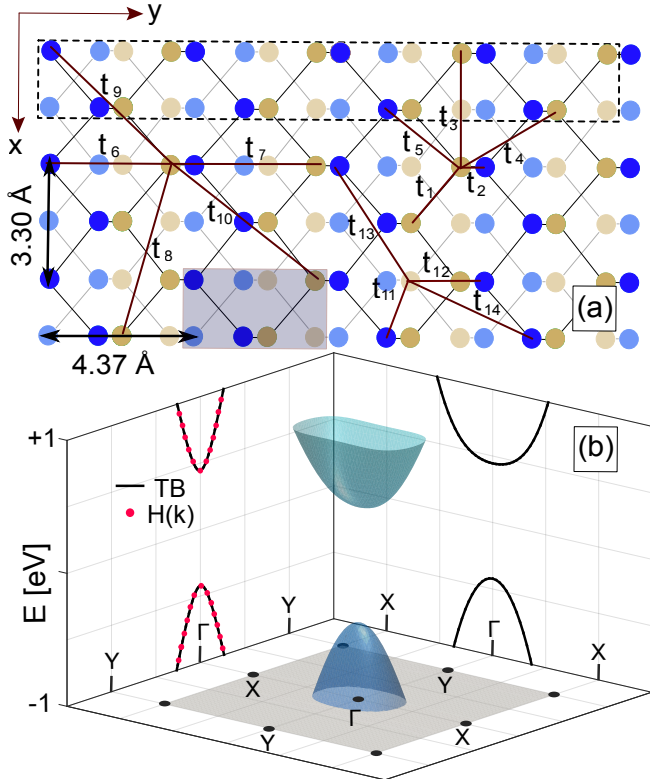


FIG. 1. (a) Schematic of bilayer phosphorene (top view). The left edge is zigzag and the right edge is beard, while the top and bottom edges are armchair. Yellow (blue) circles are the phosphorene atoms in the upper (lower) sublayer. The gray rectangle denotes the unit cell of bilayer phosphorene. Higher multilayer systems will have the same top view and with additional 4 atoms per layer. The dashed box represent the unit cell for a zigzag-zigzag phosphorene nanoribbon. (b) Band structure of unbiased trilayer phosphorene over the first Brillouin zone. Cuts normal to (10) and (01) through the Dirac point are projected onto the side walls, with the high-symmetry  $\Gamma$ , X, and Y points denoted. The solid lines are from TB, the red dotted line from the low-energy two-band Hamiltonian (2).

band Hamiltonian as

$$H(\mathbf{k}) = \mathbf{h}(\mathbf{k}) \cdot \boldsymbol{\sigma}, \quad \mathbf{h}(\mathbf{k}) = \left[ \frac{\hbar^2 k_x^2}{2m_{c(v)}} + \frac{E_g}{2}, \hbar v_y k_y, 0 \right]. \quad (2)$$

Here,  $\boldsymbol{\sigma}$  are the Pauli matrices,  $m_c$  and  $m_v$  are the effective masses in the zigzag direction, and  $v_y = 7.4 \times 10^5 \text{ m/s}$  is the Fermi velocity in the armchair direction. In Fig. 1(b), we see that the fit from this effective two-band Hamiltonian (red dots) agrees very well with the CB and VB dispersions obtained by TB (solid curve) within  $\pm 1$  eV of midgap. Finding the dispersion for  $k_x = 0$  from the two-band Hamiltonian (2) leads to

$$E(0, k_y) = \pm \sqrt{(\hbar k_y v_y)^2 + \left( \frac{E_g}{2} \right)^2}. \quad (3)$$

TABLE I. Hopping parameters for the tight-binding Hamiltonian in Eq. (1).  $i = 1 - 10$  are intralayer and  $i = 11 - 14$  are interlayer coupling terms.

$i$	$t_i$ (eV)	$d_i$ (Å)	$i$	$t_i$ (eV)	$d_i$ (Å)	$i$	$t_i$ (eV)	$d_i$ (Å)
1	-1.486	2.22	6	+0.186	4.23	11	+0.524	3.60
2	+3.379	2.24	7	-0.063	4.37	12	+0.180	3.81
3	-0.252	3.31	8	+0.101	5.18	13	-0.123	5.05
4	-0.071	3.34	9	-0.042	5.37	14	-0.168	5.08
5	-0.019	3.47	10	+0.073	5.49			

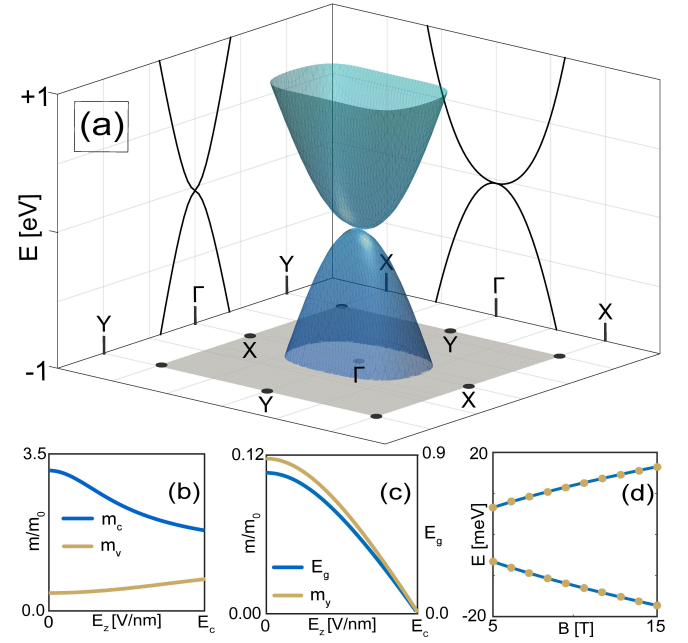


FIG. 2. (a) Band structure of biased trilayer phosphorene at the critical electric field ( $E_z = E_c$ ). (b) Effective mass in the conduction and valence bands as a function of electric field along the zigzag direction. (c) Band gap and relativistic effective mass (both CB and VB) in the armchair direction versus electric field. (d) Energy of the lowest Landau level in the CB and VB versus magnetic field  $B$ , obtained by solving Harper's equation (dots). Solid lines are fits based on Eq. (5).

This is a characteristic dispersion of massive relativistic particles [13], where  $E_g$  plays the role of rest energy. Employing the relativistic definition of the effective mass as  $m_y = \hbar^2 k (dE/dk_y)^{-1}$ , we obtain an effective mass for both CB and VB in the armchair direction to be  $m_y = E_g/2v_y^2 = 0.12m_0$ , a value close to the experimentally obtained  $0.08m_0$  [8], which could not be explained based on the parabolic approximation. Thus, it is important to consider electrons in the armchair direction as massive Dirac fermions.

*Applying vertical electric field. Critical field.* Next, we extend our model to the case of a vertical electric field  $E_z$  [applied normal to the layers, i.e., in the  $z$ -direction in Fig. 1(a)]. In the TB calculations,  $E_z$  is accounted for

by assuming a linear potential drop across the structure extending from  $-h/2$  to  $h/2$  ( $h$  is the thickness): a potential energy  $V_i = eE_z(-h/2 + z_i)$  is added to the diagonal terms of the TB Hamiltonian in Eq. (1) according to  $i$ -th atom's  $z$  coordinate. Figure 2(c) shows that, as  $E_z$  increases, the CB and VB shift toward each other due to the Stark effect. The band gap closes at a critical electric field,  $E_c$  [8], which decreases with increasing number of layers:  $E_c \simeq 0.17$  V/Å for bilayer (also reported by [14]) and  $E_c \simeq 0.15$  V/Å for trilayer phosphorene. The full band structure of trilayer phosphorene at  $E_c$  is depicted in Fig. 2(a). Electric field affects the curvature of the parabolic CB and VB bands along the zigzag direction [Fig. 2(b)]:  $m_c$  ( $m_v$ ) decreases (increases) with increasing  $E_z$ , but  $m_v < m_c$  for all values of  $E_z$ , in keeping with the high hole mobility reported in experiment [2].

Application of the vertical electric field and the corresponding gap reduction have a strong effect on dispersion in the armchair direction: as  $m_y \propto E_g$ ,  $m_y$  drops with increasing  $E_z$  and reaches zero at  $E_c$  [Fig. 2(c)]. Therefore, there is a smooth transition from massive to massless Dirac fermions in the armchair direction under a vertical electric field. At  $E_c$ , the dispersion of CB and VB near the gap becomes

$$E(\mathbf{k}) = \pm \sqrt{(\hbar k_y v_y)^2 + \left(\frac{\hbar^2 k_x^2}{2m_{c(v)}}\right)^2}. \quad (4)$$

Owing to the anisotropic dispersion at the critical electric field – massless Dirac [Eq. (4)] along  $y$ , parabolic along  $x$  – the electron density of states (DOS) has a peculiar energy dependence:  $\rho(E) \sim \frac{m}{v_y} \sqrt{E}$  [15]. If such an electron system were placed in a uniform vertical magnetic field  $B$ , it would exhibit a unique dependence of the Landau-level (LL) energy on the  $B$  field (stemming from the square-root energy dependence of the DOS [16]) that has never before been observed in experiment:

$$E_n \sim \left[ \left( n + \frac{1}{2} \right) B \right]^{2/3}, \quad (5)$$

We obtained this dependence [see Fig. 2(d)] based on solving the Harper equation [17–20]. The  $2/3$ -power dependence is distinct from the linear dispersion in two-dimensional electron gases,  $E_n \sim (n + \frac{1}{2}) B$ , and from the square-root dependence characteristic of Dirac fermions,  $E_n \sim \sqrt{(n + \frac{1}{2}) B}$ . Biased multilayer phosphorene would be the first realization of this LL dispersion in a real material, though the phenomenon was thoroughly investigated on a parametric honeycomb lattice [21–23]. While Yaun *et al.* [14] recently investigated LLs in perpendicular electric fields, they did not solve the Harper equation [17–20] in an extended system, as we did, and thus did not note this peculiar behavior at  $E_c$ . We propose an extension to experiment [8], where the gap is closed via doping and mimics applying  $E_c$ : a measurement of the Hall conductance at this condition would

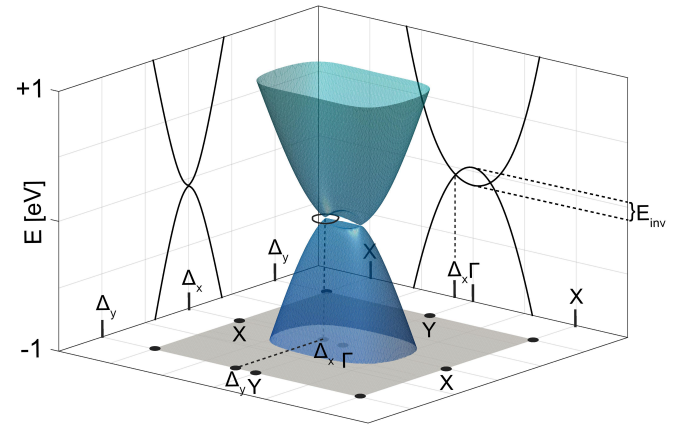


FIG. 3. Band structure of biased trilayer phosphorene at  $E_z > E_c$ . A pair of Dirac points appear in the band structure ( $\Delta_x$ ).

experimentally confirm the peculiar form (5) of the LL  $B$ -field dependence.

*Beyond the critical electric field.* Increasing the electric field beyond the critical value ( $E_z > E_c$ ) splits the Dirac point into two. The Dirac points ( $\Delta_x$ ) move away from the  $\Gamma$  point along the  $X$  direction as a function of electric field (see Fig. 3). In the low-energy, two-band Hamiltonian (2),  $\mathbf{h}(\mathbf{k})$  takes the form

$$\mathbf{h}(\mathbf{k}) = \left[ \frac{\hbar^2 k_x^2}{2m_{c(v)}} - \frac{E_{inv}}{2}, \hbar v_y k_y, 0 \right], \quad (6)$$

where  $E_{inv}$  is the value of the inverted gap shown in Fig. 3. At each Dirac point, the Hamiltonian can be expanded in terms of  $\mathbf{q} = \mathbf{k} - \mathbf{k}_{\Delta_x}$ , which gives us the low-energy form  $H(\mathbf{q}) = \hbar v_x q_x + \hbar v_y q_y$ , a generic Dirac Hamiltonian with anisotropic Fermi velocity  $v_{x,c(v)} = \sqrt{E_{inv}/m_{c(v)}}$  and ultimately the dispersion relation

$$E(\mathbf{q}) = \sqrt{(\hbar v_x q_x)^2 + (\hbar v_y q_y)^2} \quad (7)$$

Based on this dispersion, the Berry phase,  $\Lambda$ , can be calculated by integrating the Berry potential,  $\nabla \Lambda = \frac{\hbar^2 v_x v_y}{2E(\mathbf{q})^2} [-q_y, q_x]$ , over a closed path around each Dirac point; the integration path chosen here is a circle around each Dirac point, depicted in Fig. 3.  $\Lambda = \pi$  is obtained from both the two-band low-energy and TB Hamiltonians [24, 25]. This means that electrons in biased multilayer phosphorene carry an extra degree of freedom called the pseudospin, and are expected to exhibit unconventional quantum Hall effect, where Landau levels vary with  $B$  as  $E_n \sim \sqrt{(n + \frac{1}{2}) B}$  [14, 26].

*Multilayer phosphorene nanoribbons (PNRs). Midgap bands and edge states.* We confine multilayer phosphorene along the armchair direction, with both edges

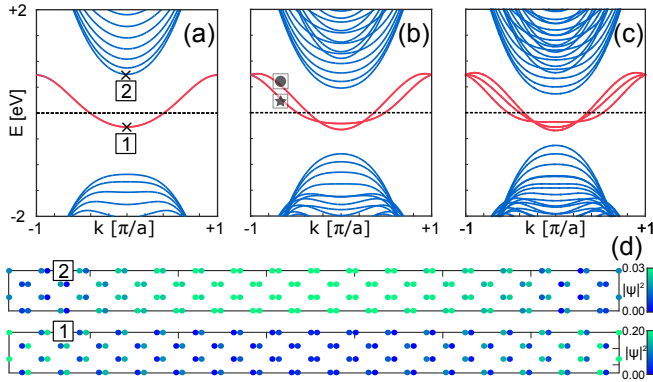


FIG. 4. Band structure of (a) monolayer, (b) bilayer, and (c) trilayer zigzag PNRs, each 7 nm wide. (d) Real-space probability density distributions for the two  $k = 0$  wave functions marked in panel (a).

terminated by the zigzag arrangement; this quasi-one-dimensional structure is a zigzag PNR. The band structures of mono-, bi-, and trilayer PNRs are shown in Figs. 4(a)-(c). One can see the presence of midgap bands (red curves) completely detached from the bulk states (shown in blue). Each layer of phosphorene contributes one band of twofold-degenerate midgap states, making a total of two, four, six midgap states for mono-, bi- and trilayer PNRs, respectively. (Only zigzag PNRs have degenerate midgap bands.)

In the absence of a vertical electric field, the Fermi level passes through the midgap bands and is far from the bulk states. Therefore, near-equilibrium electronic transport in PNRs is governed by midgap states. In Fig. 4(d), we plot the probability density for two  $k = 0$  wave functions marked in Fig. 4(a), one from a midgap band (denoted by 1) and another from the bulk CB (denoted by 2). In contrast to the state 2 from the bulk band, whose probability density peaks near the PNR middle, the midgap state's probability density is highest by the edges (near one edge in the top and near the other in the bottom sublayer of a monolayer). Therefore, electronic transport in PNRs should be tunable by the manipulation of the midgap states, confined to the edges.

Based on this finding, we propose a field-effect-transistor (FET) structure shown in Fig. 5(a), where the conductance in PNRs via the midgap states (which are confined near the edges) is modulated locally by two edge gates, with voltages  $V_{g1}$  and  $V_{g2}$ . A 28-nm-wide bilayer PNR is chosen, wide enough for experimental realization yet narrow enough to be computationally feasible via atomistic TB and nonequilibrium Green's functions (NEGF) [27]. The width of each edge gate is 8.3 nm. Figure 5(b) shows the band dispersion for  $V_{g1} = -V_{g2} = +0.4V$ . The applied bias strongly affects the midgap states that have a high probability density right under the gate and shifts two bands upward and

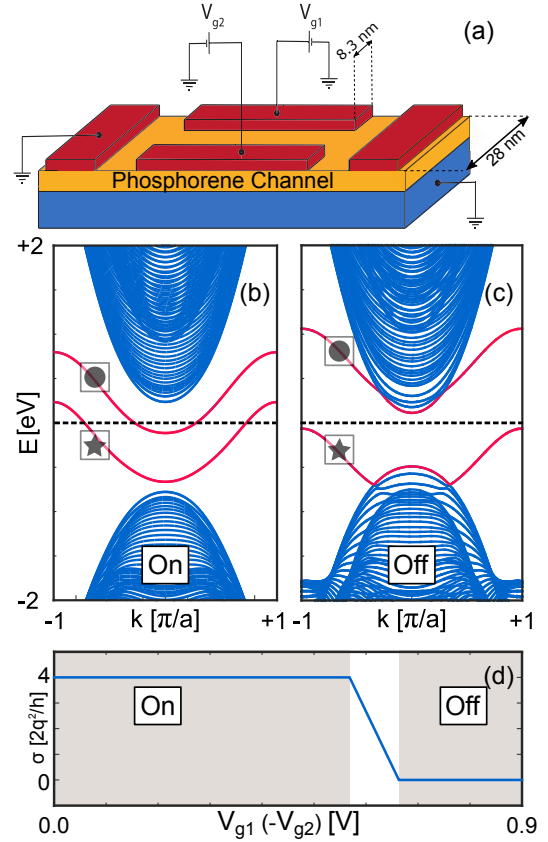


FIG. 5. (a) Schematic of the proposed edge-gate field-effect structure to control the conductance in PNRs. (b) & (c) Band structure of bilayer PNRs under applied bias on the edge gates: (b)  $V_{g1} = -V_{g2} = +0.4V$  and (c)  $V_{g1} = -V_{g2} = +0.8V$ . Red curves represent the dispersions of four midgap bands (two twofold degenerate bands, denoted by circle and star in Fig. 4), whose wave functions are confined near the PNR edges. The dashed horizontal line represents the Fermi level. (c) Conductance of bilayer PNR as a function of applied bias on the edge gates, showing a transition from “on” to “off.”

other two downward, preserving the twofold degeneracy. These edge gates have essentially no effect on the bulk bands. Although the midgap states have moved toward the bulk bands compared to their initial position in the gap [see Fig. 5(b)], the ribbon remains metallic since the Fermi level [which is fixed by the potentials on the source and drain on the left and right, Fig. 5(a)] still passes through the midgap bands. Increasing the bias voltages to  $V_{g1} = -V_{g2} = +0.8V$  in Fig. 4(c) leads to a further energy separation of the midgap bands, so there are no states at the Fermi level, which denotes a transition from conducting [Fig. 5(b)] to insulating behavior [Fig. 5(c)], as demonstrated by calculating the conductance  $\sigma$  [Fig. 5(d)] using the NEGF formalism [27].

At low bias on the edge gates, the conductance  $\sigma$  [Fig. 5(d)] at the Fermi energy is  $8e^2/h$ , indicating four total conducting channels from the two twofold-degenerate

states at the Fermi level [see Fig. 4(b)]. As the voltage magnitude increases, the midgap states are pushed apart. Above a threshold bias on the edge gates (around 0.7 V here, but dependent on the ribbon and gate widths), the conductance becomes zero [Fig. 5(d)]. This dual-edge-gate structure is compatible with current fabrication technology, as similar multigate structures were realized previously [28, 29]. Also, the topologically protected midgap states are robust against bulk vacancies [30]. A recent calculation showed that edge functionalization can lead to a dramatic flattening of the midgap-band dispersions [31], which would significantly reduce the threshold voltage required for the “on”-to-“off” transition.

In summary, we showed that the electron band dispersion for multilayer phosphorene transitions from parabolic in the zigzag and massive Dirac fermion in the armchair direction at vertical electric fields below  $E_c$  to a dispersion of an anisotropic massless Dirac fermion at electric fields above  $E_c$ . We posited that this transition would be observed in quantum Hall experiments as an electric-field-dependent change in the Landau-level energy vs  $B$ :  $\sim (n + 1/2)B$  below  $E_c$ ,  $\sim [(n + 1/2)B]^{2/3}$  at  $E_c$ , and  $\sim [(n + 1/2)B]^{1/2}$  above  $E_c$ . Moreover, we showed that PNRs feature edge states with energies belonging to midgap bands (degenerate in zigzag PNRs), which govern low-field conduction. We proposed a structure with dual edge gates that strongly affect the edge states but leave the bulk ones inert. The dual-edge-gate structure can induce a transition from a conducting “on” state to an insulating “off” state by moving the midgap bands away from the Fermi level, thereby realizing field-effect transistor action on PNRs. Electric-field modulation of phosphorene and PNRs is a versatile concept that can enable access to new physics and establish a framework for further investigation of phosphorene-based devices.

- [8] J. Kim, S. S. Baik, S. H. Ryu, Y. Sohn, S. Park, B.-G. Park, J. Denlinger, Y. Yi, H. J. Choi, and K. S. Kim, *Science* **349**, 723 (2015).
- [9] F. Xia, H. Wang, and Y. Jia, *Nat. Commun.* **5**, 4458 (2014).
- [10] S. Yuan, A. N. Rudenko, and M. I. Katsnelson, *Phys. Rev. B* **91**, 115436 (2015), URL <http://link.aps.org/doi/10.1103/PhysRevB.91.115436>.
- [11] T. Low, R. Roldán, H. Wang, F. Xia, P. Avouris, L. M. Moreno, and F. Guinea, *Phys. Rev. Lett.* **113**, 106802 (2014), URL <http://link.aps.org/doi/10.1103/PhysRevLett.113.106802>.
- [12] A. Rudenko, S. Yuan, and M. Katsnelson, *Phys. Rev. B* **92**, 085419 (2015).
- [13] S. Weinberg and R. Dicke, *American Journal of Physics* **41**, 598 (1973).
- [14] S. Yuan, E. van Veen, M. I. Katsnelson, and R. Roldán, *Phys. Rev. B* **93**, 245433 (2016), URL <http://link.aps.org/doi/10.1103/PhysRevB.93.245433>.
- [15] Y. Hasegawa, R. Konno, H. Nakano, and M. Kohmoto, *Phys. Rev. B* **74**, 033413 (2006).
- [16] The condition for energy levels in a magnetic field  $B$  is  $S(E) = 2\pi(n + \frac{1}{2})eB$ , where  $S(E)$  is the area of the constant-energy surface in reciprocal space [32]. Since  $\rho(E) \sim \frac{\partial S(E)}{\partial E}$ , the Landau levels are found to be  $E_n \sim [(n + \frac{1}{2})B]^{2/3}$  for multilayer phosphorene at the critical field.
- [17] P. G. Harper, *Proceedings of the Physical Society. Section A* **68**, 874 (1955), URL <http://stacks.iop.org/0370-1298/68/i=10/a=304>.
- [18] D. J. Thouless, M. Kohmoto, M. P. Nightingale, and M. den Nijs, *Phys. Rev. Lett.* **49**, 405 (1982), URL <http://link.aps.org/doi/10.1103/PhysRevLett.49.405>.
- [19] K. Wakabayashi, M. Fujita, H. Ajiki, and M. Sigrist, *Phys. Rev. B* **59**, 8271 (1999), URL <http://link.aps.org/doi/10.1103/PhysRevB.59.8271>.
- [20] P. B. Wiegmann and A. V. Zabrodin, *Phys. Rev. Lett.* **72**, 1890 (1994), URL <http://link.aps.org/doi/10.1103/PhysRevLett.72.1890>.
- [21] P. Dietl, F. Piéchon, and G. Montambaux, *Phys. Rev. Lett.* **100**, 236405 (2008).
- [22] G. Montambaux, F. Piéchon, J.-N. Fuchs, and M. O. Goerbig, *Phys. Rev. B* **80**, 153412 (2009).
- [23] G. Montambaux, F. Piéchon, J.-N. Fuchs, and M. Goerbig, *The European Physical Journal B* **72**, 509 (2009).
- [24] C.-H. Park and N. Marzari, *Phys. Rev. B* **84**, 205440 (2011).
- [25] R. Resta, *Journal of Physics: Condensed Matter* **12**, R107 (2000).
- [26] Y. Zhang, Y.-W. Tan, H. L. Stormer, and P. Kim, *Nature* **438**, 201 (2005).
- [27] S. Datta, *Electronic transport in mesoscopic systems* (Cambridge university press, 1997).
- [28] M. Craciun, S. Russo, M. Yamamoto, J. B. Oostinga, A. Morpurgo, and S. Tarucha, *Nature Nano* **4**, 383 (2009).
- [29] J. Williams, T. Low, M. Lundstrom, and C. Marcus, *Nature Nano* **6**, 222 (2011).
- [30] M. Ezawa, *New Journal of Physics* **16**, 115004 (2014).
- [31] X. Peng, A. Copple, and Q. Wei, *Journal of Applied Physics* **116**, 144301 (2014).
- [32] I. Lifshitz and A. M. Kosevich, *Soviet Physics JETP-USSR* **2**, 636 (1956).

\* irena.knezevic@wisc.edu

- [1] W. Lu, H. Nan, J. Hong, Y. Chen, C. Zhu, Z. Liang, X. Ma, Z. Ni, C. Jin, and Z. Zhang, *Nano Research* **7**, 853 (2014).
- [2] H. Liu, A. T. Neal, Z. Zhu, Z. Luo, X. Xu, D. Tománek, and P. D. Ye, *ACS Nano* **8**, 4033 (2014).
- [3] S. Zhang, J. Yang, R. Xu, F. Wang, W. Li, M. Ghufran, Y.-W. Zhang, Z. Yu, G. Zhang, Q. Qin, et al., *ACS Nano* **8**, 9590 (2014), pMID: 25188827, <http://dx.doi.org/10.1021/nn503893j>, URL <http://dx.doi.org/10.1021/nn503893j>.
- [4] M. Elahi, K. Khaliji, S. M. Tabatabaei, M. Pourfath, and R. Asgari, *Phys. Rev. B* **91**, 115412 (2015).
- [5] R. Fei and L. Yang, *Nano Lett.* **14**, 2884 (2014).
- [6] R. Fei, A. Faghaninia, R. Soklaski, J.-A. Yan, C. Lo, and L. Yang, *Nano Lett.* **14**, 6393 (2014).
- [7] S. Das, W. Zhang, M. Demarteau, A. Hoffmann, M. Dubey, and A. Roelofs, *Nano Lett.* **14**, 5733 (2014).